12-7-2016

Over or Under: Hydride Attack at the Metal versus the Coordinated Nitrosyl Ligand in Ferric Nitrosyl Porphyrins.

E G. Abucayon
University of Oklahoma

R L. Khade
Stevens Institute of Technology

D R. Powell
University of Oklahoma

Michael J. Shaw
Southern Illinois University at Edwardsville, michsha@siue.edu

Y Yang
Stevens Institute of Technology

See next page for additional authors

Authors
E G. Abucayon, R L. Khade, D R. Powell, Michael J. Shaw, Y Yang, and G B. Richter-Addo

Cover Page Footnote
This is the Accepted Manuscript version of an article published in *Dalton Transactions* on December 7, 2016.

Dalton Transactions

ARTICLE

Over or under: Hydride attack at the metal versus the coordinated nitrosyl ligand in ferric nitrosyl porphyrins†

Received 00th January 20xx,
Accepted 00th January 20xx

DOI: 10.1039/x0xx00000x

www.rsc.org/

E. G. Abucayon,[a] R. L. Khade,[b] D. R. Powell,[a] M. J. Shaw,[c] Y. Zhang,*[b] and G. B. Richter-Addo*[a]

Hydride attack at a ferric heme–NO to give an Fe–HNO intermediate is a key step in the global N-cycle. We demonstrate differential reactivity when six- and five-coordinate ferric heme-NO models react with hydride. Although Fe–HNO formation is thermodynamically favored from this reaction, Fe–H formation is kinetically favored for the 5C case.

Introduction

Nitroxyl (HNO) is gaining attention as a significant player in the overall biology of nitric oxide (NO) due to its involvement as a reactive intermediate in the global N-cycle.[1-4] HNO can be generated by metal-mediated and organic processes.[5, 6] Heme–HNO species are present in the reaction cycles of cyt *c* nitrite reductases (via proton attack on a heme-bound NO),[7] and in fungal cyt P450 NO reductases (via hydride attack on a ferric heme–NO) en route to N_2O formation.[8] Very little experimental information on heme model-HNO compounds is available.[1-4, 9-12] Farmer and coworkers have reported the spectroscopic characterization of several heme protein-HNO adducts.[13] Coordination non-heme compounds with HNO ligands have been reviewed.[1, 2, 14] Related anionic (i.e., non-protonated) synthetic porphyrin-NO compounds of the form $[(por)Fe(NO)]^-$ [9, 10, 12, 15] have been characterized, and two such species, namely $[(TFTTBr_8)Fe(NO)]^-$ ($TFTTBr_8$ = octabromo[tetrakis(pentafluorophenyl)porphyrinato dianion) [16] and $[(OEP)Fe(NO)]^-$ (OEP = octaethylpoprhyrinato dianion)[17] have been structurally characterized by X-ray crystallography. Although density functional theory (DFT) calculations have aided significantly in our theoretical understanding of heme–HNO compounds, [3, 7, 18-20] the general lack of appropriate experimental heme–HNO models has hindered research in this important area.

We recently reported that hydride attack at the coordinated NO group in a ferric $[(OEP)Fe(NO)(5\text{-MeIm})]^+$ compound generates the Fe–HNO derivative (eq 1),[21] modeling a key step in cyt P450nor catalysis. Of prime importance is an examination of factors that lead to successful hydride attack at

$$[(OEP)Fe(NO)(5\text{-MeIm})]^+ + H^- \rightarrow (OEP)Fe(HNO)(5\text{-MeIm}) \quad (1)$$

the coordinated NO of ferric–NO hemes. The availability of both six-coordinate and five-coordinate ferric–NO heme models has allowed us to investigate hydride attack at the coordinated NO and/or the Fe center experimentally and computationally (e.g., the 5C case shown in eq 2).

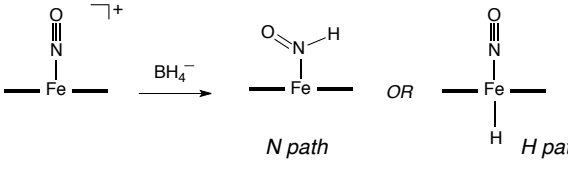

(2)

Results and discussion

Following up on our earlier report, we have determined that the attack of hydride at the coordinated NO groups of six-coordinate cationic ferric-NO heme models can be quite general. In this work, we prepared several $[(por)Fe(NO)(L)]+$ compounds (por = dianions of protoporphyrin IX dimethyl ester (PPDME), OEP, and TTP (tetratolylporphyrin)). The crystal structure of $[(PPDME)Fe(NO)(5\text{-MeIm})]SbF_6$, an excellent model for histidine-ligated (PPIX)Fe, is shown in Fig. 1.‡

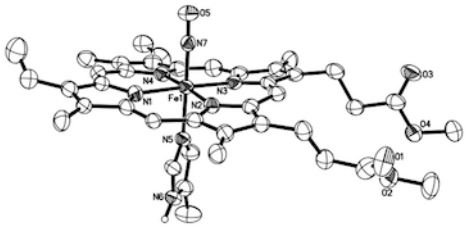

Fig. 1. Molecular structure of the cation of $[(PPDME)Fe(NO)(5\text{-MeIm})]SbF_6$ in the $P\bar{1}$ space group (with thermal ellipsoids drawn at 50%). The H atoms (except for the imidazole N6 proton) and the anion have been omitted for clarity. Fe1–N7 = 1.654(5) Å, N7–O5 = 1.133(6) Å, Fe1–N5 = 1.990(5), ∠Fe1–N7–O5 = 174.8(5)°.

[a] Department of Chemistry and Biochemistry, University of Oklahoma, Norman, Oklahoma 73019, United States.
[b] Department of Biomedical Engineering, Chemistry and Biological Sciences, Stevens Institute of Technology, Castle Point on Hudson, Hoboken, New Jersey, 07030, United States.
[c] Department of Chemistry, Southern Illinois University Edwardsville, Edwardsville, Illinois 62025, United States.

Electronic Supplementary Information (ESI) available: Experimental, X-ray, and computational details. See DOI: 10.1039/x0xx00000x

The reactions of these cations with borohydride (as the source of hydride) are best carried out at low temperature (–35 to –20 °C), as the products decompose readily at higher temperatures. For example, with the reaction $[(PPDME)Fe(NO)(1\text{-MeIm})]^+$ cation (υ_{NO} 1915 cm^{-1}) with borohydride generates the (PPDME)Fe(HNO)(1-MeIm) product characterized by a new band in its IR spectrum at 1384 cm^{-1} assigned to the υ_{NO} of the newly-formed Fe–HNO group (Fig. 2). This Fe–HNO decomposes even at this temperature to the paramagnetic (PPDME)Fe(NO) species (υ_{NO} 1672 cm^{-1}) (see later).

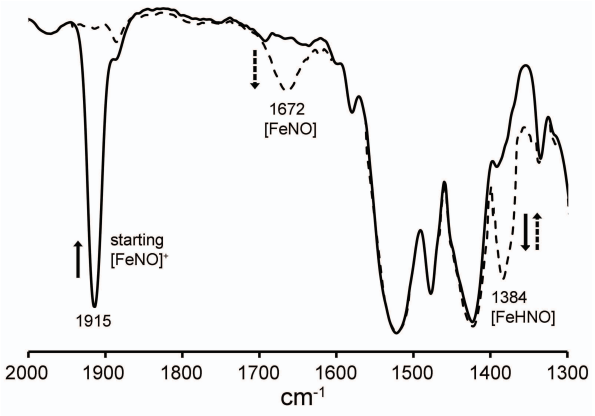

Fig. 2 IR spectroscopic characterization of the bound HNO ligand in (PPDME)Fe(HNO)(1-MeIm), showing formation of the υ_{NO} 1384 cm^{-1} band (dashed line) upon hydride addition to the cationic precursor (υ_{NO} 1915 cm^{-1}). The new 1384 cm^{-1} band slowly converts to the band at 1672 cm^{-1}.

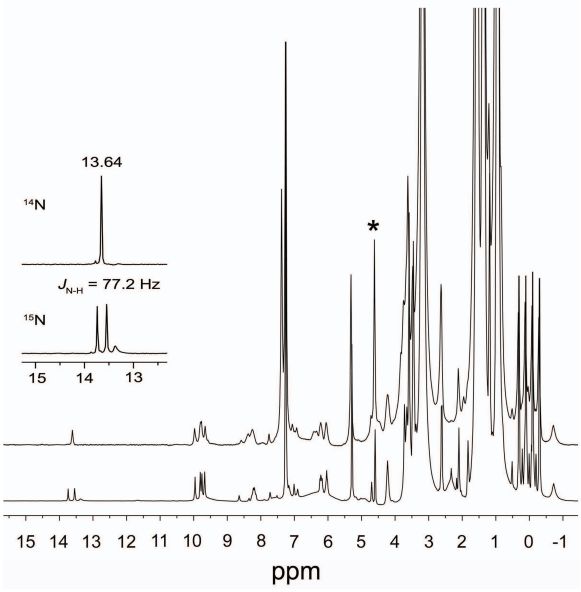

Fig. 3. ^1H NMR spectra (in $CDCl_3$) of the reaction of $[(PPDME)Fe(NO)(1\text{-MeIm})]OTf$ with $[NBu_4]BH_4$ to generate (PPDME)Fe(HNO)(1-MeIm). The bottom spectrum showing the splitting of the Fe-HNO peak at 13.64 ppm into a doublet was obtained using $[(PPDME)Fe(^{15}NO)(1\text{-MeIm})]OTf$ in the reaction. The peak labeled * is due to the H_2 decomposition product (see text and Fig. S2).

The generated (PPDME)Fe(HNO)(1-MeIm) product is also characterized by a singlet peak at 13.64 ppm in the ^1H NMR spectrum that splits into a doublet (J_{NH} 77 Hz) with ^{15}NO labeling (Fig. 3). The ^1H NMR spectra from the related reaction to generate the (PPDME)Fe(HNO)(5-MeIm) analogue are shown in Fig. S1a. The low-temperature IR and ^1H NMR spectral data for these and other Fe–HNO compounds prepared in this work are collected in Table 1.

Table 1. Spectral data for the precursor $[(por)Fe(NO)(L)]^+$ and (por)Fe(HNO)(L) complexes.[a]

		$[(por)Fe(NO)L]^+$	(por)Fe(HNO)(L)	
por	L	IR (cm^{-1})	IR (cm^{-1})	^1H NMR, ppm[b]
OEP	ImH	1911	1381	13.93 (78)
	5-MeIm	1910	1383	13.99 (76)
	1-MeIm	1912	1388	13.72 (77)
PPDME	ImH	1915	1382	13.90 (76)
	5-MeIm	1912	1382	13.93 (77)
	1-MeIm	1915	1384	13.65 (77)
TTP	ImH	1917	1386	14.20 (76)
	5-MeIm	1912	1381	14.26 (76)
	1-MeIm	1914	1389	14.02 (76)

[a] IR data in $CHCl_3$ (at –45 °C), and ^1H NMR data in $CDCl_3$ (at –20 °C). [b] The $J_{N\text{-}H}$ coupling constants (in Hz) for the $Fe(H^{15}NO)$ derivatives are in brackets.

The spectral data for the Fe–HNO complexes are reproduced well by DFT calculations using both the pyrrole-substituted (OEP) and *meso*-substituted (TTP) porphyrins, and an N-substituted imidazole (1-MeIm) and the histidine mimic (5-MeIm). Our experimental observations of a mild effect of OEP vs. TTP macrocycle and axial ligand (5-MeIm vs. 1-MeIm) type on ^1H NMR chemical shifts (range of 0.54 ppm; ~4%), but essentially negligible (<1%) υ_{NO} shifts for these systems, are reproduced by the calculations (Table S1); with range of proton shifts of 0.69 ppm (~5%) and range of υ_{NO} shifts of <1%, affirming that ^1H NMR spectroscopy is a more sensitive structural probe for these Fe–HNO systems.

In contrast, the reaction of borohydride with the five-coordinate $[(OEP)Fe(NO)]OTf$ (Fig. 4)‡ at –35 °C does not result

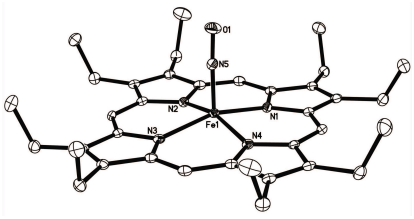

Fig. 4. Molecular structure of the cation of $[(OEP)Fe(NO)]OTf$ in the $P\bar{1}$ space group (with thermal ellipsoids drawn at 50%). The H atoms (except for the imidazole N6 proton) and the anion have been omitted for clarity. Fe1–N5 = 1.6371(15) Å, N5–O1 = 1.1473(19) Å, ∠Fe1–N5–O1 = 176.15(15)°. The related $[(OEP)Fe(NO)]ClO_4$ structure in the $P2_1/n$ space group has been reported.[22, 23]

in new ^{15}N isotope sensitive peaks in the 11–15 ppm region of the ^1H NMR spectrum attributable to an Fe–HNO derivative. Rather, a new sharp peak at –4.11 ppm is observed that we attribute to the six-coordinate Fe-hydride product

(OEP)Fe(NO)H (Fig. 5a). Importantly, the DFT-calculated ^{1}H NMR chemical shift of the hydride peak for (OEP)Fe(NO)H is at –3.64 ppm, which is in good agreement with the experimentally observed value of –4.11 ppm.

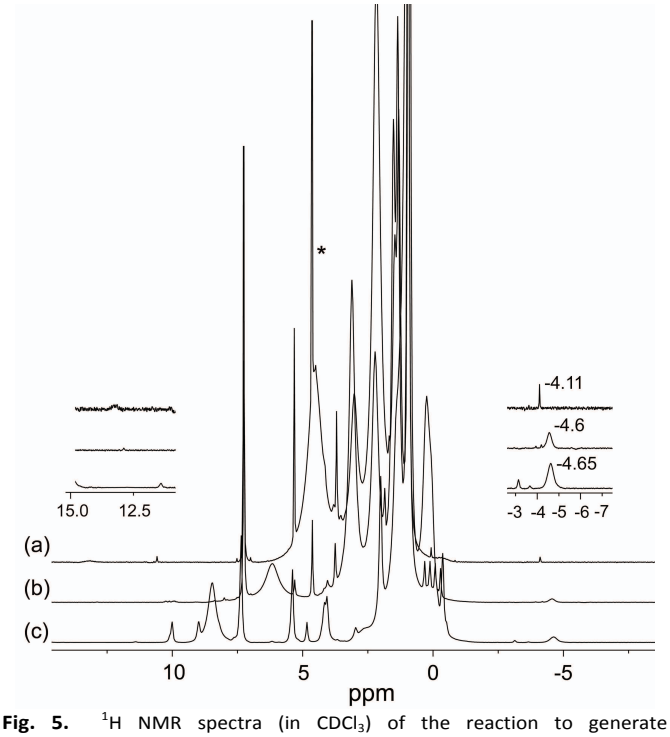

Fig. 5. ^{1}H NMR spectra (in $CDCl_3$) of the reaction to generate (OEP)Fe(NO)H, highlighting the upfield and downfield regions of (a) (OEP)Fe(NO)H (top spectrum), (b) (OEP)Fe(H) byproduct (middle spectrum), and (c) (OEP)Fe(H) from the control reaction of [(OEP)Fe]OTf with hydride (bottom spectrum). The peak labeled * is due to the H_2 decomposition product (see text).

Interestingly, geometry optimization of the model (porphine)Fe(NO)H product reveals a core geometry not unlike that of the structurally characterized aryl derivative (OEP)Fe(NO)(C_6H_4F-*p*),[24] showing an off-axis tilt of the nitrosyl N atom, a bent FeNO moiety (∠FeNO = 155.2°), and an asymmetry of the equatorial Fe–N(por) core displaying longer Fe–N(por) distances in the direction of the bent FeNO moiety (Fig. 6).

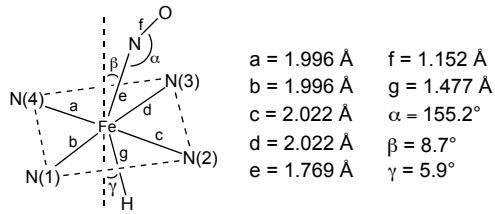

Fig. 6. Selected geometrical parameters (in Å and degrees) for DFT-calculated (OEP)Fe(NO)H. The tilting angles are with respect to the four-nitrogen porphyrin plane.

We observe, on occasion, an additional broad peak at –4.6 ppm in the ^{1}H NMR spectrum (Fig. 5b). We attribute this latter peak to the non-nitrosyl paramagnetic (OEP)Fe(H) compound, probably resulting from dissociation of NO from the ferric $[(OEP)Fe(NO)]^+$ cation in solution prior to hydride attack. Indeed, a control experiment involving the reaction of $[(OEP)Fe]^+$ with borohydride reproduces this peak (Fig. 5c).

The (OEP)Fe(NO)H product is very unstable even at –35 °C, with the Fe-*H* peak at –4.11 ppm in the ^{1}H NMR spectrum disappearing even after only ~15 mins. In fact, this peak is not detectable in the ^{1}H NMR spectrum when the reaction is carried out at –20 °C. The (OEP)Fe(NO)H decomposition products are (OEP)Fe(NO) (87% total yield by IR) and H_2 (85% total yield by NMR). That diborane is the boron-containing by-product in both the reactions of the six-coordinate $[(OEP)Fe(NO)(5\text{-MeIm})]^+$ and five-coordinate $[(OEP)Fe(NO)]^+$ with borohydride was verified by $^{11}B\{^{1}H\}$ NMR spectroscopy (Fig. 7), which showed identical ^{11}B NMR signals at –26 ppm when compared with that of authentic diborane (prepared from the reaction of borohydride with a reactive alkyl halide).[25]

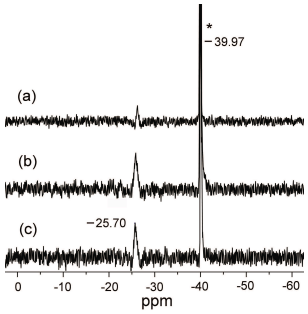

Fig. 7. $^{11}B\{^{1}H\}$ NMR spectra of the product mixtures from (a) the reaction of [(OEP)Fe(NO)(5-MeIm)]OTf with excess $[NBu_4]BH_4$ (signal at –40 ppm), and (b) the reaction of [(OEP)Fe(NO)]OTf with excess $[NBu_4]BH_4$, and (c) the control and known reaction of $[NBu_4]BH_4$ with 1,2-dichloroethane to generate diborane.[25]

We employed DFT calculations to provide insight into the differential Fe–H versus Fe–HNO bond-forming reactions (Scheme 1) when the five-coordinate $[(porphine)Fe(NO)]^+$ cation (**R1**) is reacted with borohydride (**R2**). We previously reported the calculated reaction path for the analogous six-coordinate compound $[(porphine)Fe(NO)(5\text{-MeIm})]^+$.[21] The "N path" in Scheme 1 represents an attack of hydride at the coordinated NO, and the "H path" represents direct Fe–H bond formation. The calculated electronic energies (ΔE), zero-point energy corrected electronic energies (ΔE_{ZPE}), enthalpies (ΔH), and Gibbs free energy (ΔG) follow the same trends for the N- and the H-paths (Table S2).

The first encounter intermediate in the N-path is represented by **I-1$_N$** in Scheme 1, with a distance of 2.984 Å (Table S3) between the nitrosyl N atom and the hydride to be transferred. This distance shortens to 2.441 Å in the transition state **TS$_N$**, with an accompanying very slight lengthening of the bond between boron and the hydride to be transferred. In fact, the similarity of the B–H bond lengths in **TS$_N$** and the reagent **R2**, and the large difference (of 1.405 Å) in the N–H bond lengths between that in **TS$_N$** and the final Fe–HNO product **P-1$_N$** suggests an early transition state along the N-path, as observed also for the six-coordinate systems.[21]

Dalton Transactions

ARTICLE

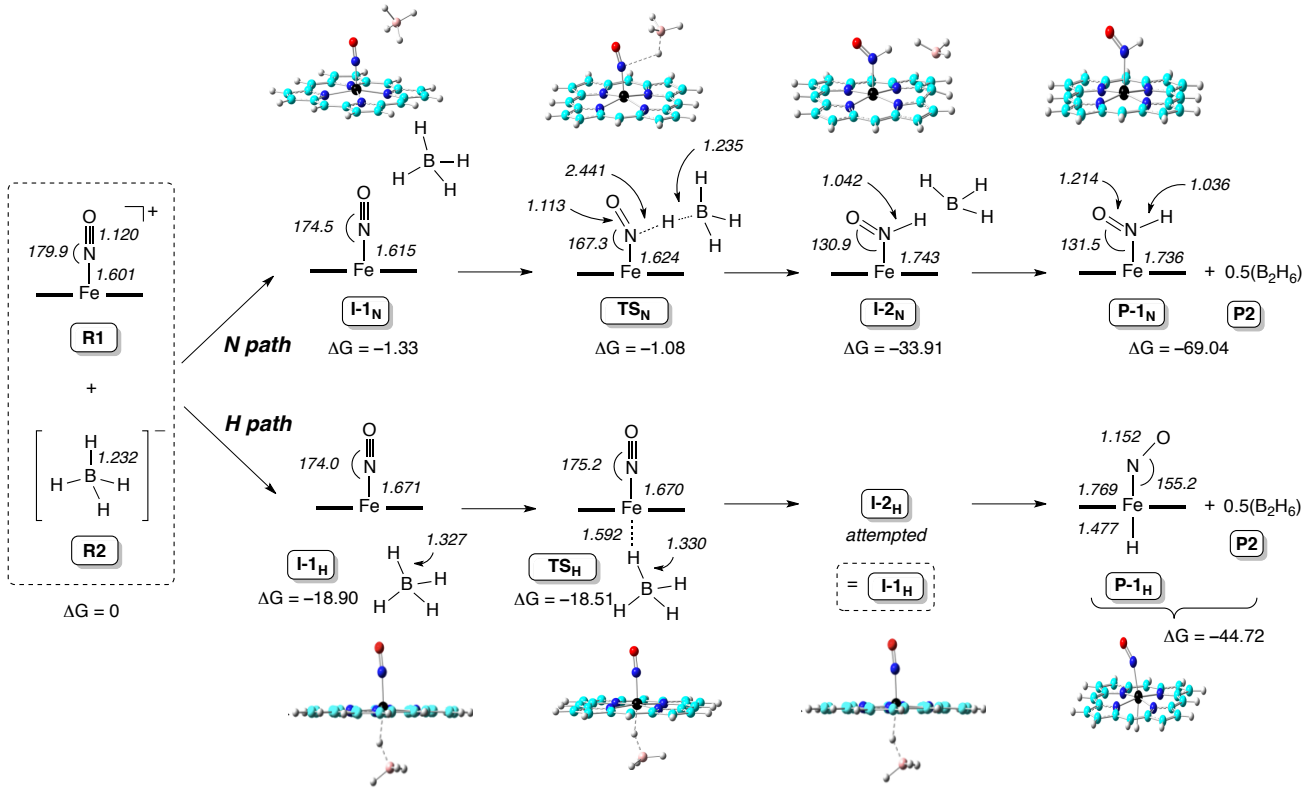

Scheme 1. DFT-calculated N- and H-pathways for hydride addition to the five-coordinate [(P)Fe(NO)]$^+$ cation.

The H-path first generates the intermediate **I-1$_H$** with a distance of 1.594 Å (Table S3) between the Fe and the hydride to be transferred; this distance is much shorter than that seen in **I-1$_N$**, suggesting a stronger Fe···HBH$_3$ interaction in **I-1$_H$** (H-path) than the N···HBH$_3$ interaction in **I-1$_N$** (N-path). This trend is also maintained in both transition states **TS$_N$** and **TS$_H$**. While the data for the N-path suggests an early transition state, that for the H-path suggests a much later transition state. For example, for the H-path, the difference in the Fe–H distances between **TS$_H$** and **P-1$_H$** is only 0.115 Å (c.f., the analogous difference in N–H distances of 1.405 Å along the N-path). Further, the difference in the B–H (H to be transferred) bond distances in **TS$_H$** and in the initial reactant **R2** is 0.098 Å, ~33x the noted difference along the related N-path. Attempts to locate a distinct second intermediate **I-2$_H$**, using a shorter Fe···H length and longer FeH···BH$_3$ distance (en route **P-1$_H$**), yielded the same **I-1$_H$** structure, probably due to the strong favorable electronic driving force between the ferric metal center and the hydride as discussed above, and the strong interaction between hydride and BH$_3$ (the B-H bond length difference between **I-1$_H$**/**I-2$_H$** and **TS$_H$** is only 0.003 Å).

Analysis of the data above shows that although *both pathways* of hydride attack on the five-coordinate [(por)Fe(NO)]$^+$ are thermodynamically favorable, the H-path is kinetically more favorable than the N-path by 17.43 kcal/mol (i.e., $\Delta E|TS_H–TS_N|$), supporting the experimental formation of the Fe–H hydride complex with no observation of the Fe–HNO product. The charge analysis data (Table S4) is also consistent with the experimental and energy results; in the precursor cation [(porphine)Fe(NO)]$^+$ (**R1**), the Fe atom bears a more positive charge (0.999e) than the nitrosyl N atom (0.101e; i.e. by ~9.9x), consistent with an easier hydride transfer to Fe rather than N. In accordance with such a strong electronic driving force difference, and based on the charge differences in transition states and reactants (Table S4), hydride transfer to Fe results in a donation of 0.652e from borohydride, while the hydride transfer to the nitrosyl N results in a much smaller donation of 0.136e from borohydride.

Both the (por)Fe(HNO)(L) (Table 1) and (OEP)Fe(NO)H systems are thermally unstable even at –35 °C. For example, although the Fe–*H*NO peaks for the (OEP)Fe(HNO)(L) compounds are persistent in the ^{1}H NMR spectra for ~2 h

(integrating to ~5-21% variable yields), the compounds decompose to generate H_2 (by ^{1}H NMR) and the five-coordinate (OEP)Fe(NO) derivative (by IR), with overall yields of 85% (L = 5-MeIm), 52% (L = ImH), and 76% (L = 1-MeIm), respectively, based on the cationic $[(OEP)Fe(NO)(L)]^+$ precursors. The analogous overall yields for the PPDME systems to give (PPDME)Fe(NO) are 41%, 65%, and 51%, respectively. We surmise that HNO dissociation from the six-coordinate (por)Fe(HNO)(imidazole) products does not occur, as N_2O (the HNO dimerization product) is not detected in the headspace gas by IR spectroscopy. Curiously, when borodeuteride is used for the reaction with the $[(OEP)Fe(NO)(5\text{-MeIm})]^+$ cationic precursor (eq 1), D_2 is similarly generated (identified by ^{2}H NMR spectroscopy) together with (OEP)Fe(NO), but we also detected the presence of N_2O (by IR) and D_2O (by ^{2}H NMR spectroscopy), indicative of *both* D–NO bond cleavage and partial DNO dissociation from the (OEP)Fe(DNO)(5-MeIm) complex. In contrast, the reaction of borodeuteride with the five-coordinate $[(OEP)Fe(NO)]^+$ cation resulted in the net formation of only D_2 and (OEP)Fe(NO).

We then employed DFT calculations to probe the Fe-HNO decomposition pathways. Selected data are shown in Fig. 8. and in Tables 2 and S5. As seen from the enthalpy costs to break the H–NO and Fe–N(H)O bonds, the covalent H–NO bond is stronger than the Fe–N(H)O coordination bond, as expected from the bonding nature, and both bonds become

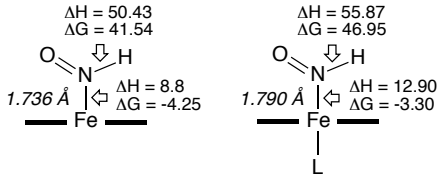

Fig. 8. Bond strength energies (ΔH and ΔG) for the five-coordinate and six-coordinate Fe–HNO systems (L = 5-MeIm). Values are in kcal/mol.

Table 2. Reaction energies (in kcal/mol).[a]

C.N.	Decomposition pathway	ΔG
5-C	(P)Fe(HNO) → (P)Fe + 1/2(N_2O + H_2O)	–48.71
5-C	(P)Fe(HNO) → (P)Fe(NO)+ 1/2 H_2	–4.78
6-C	(P)Fe(HNO)L → (P)Fe(L) + 1/2(N_2O + H_2O)	–47.76
6-C	(P)Fe(HNO)L → (P)Fe(NO) + L + 1/2 H_2	–3.19
	HNO → 1/2(N_2O + H_2O)	–44.46

[a] C.N. = coordination number. P = porphine. L = 5-MeIm.

stronger in the presence of the axial 5-MeIm ligand. Although the *trans* effect elongates the Fe–N(H)O bond length by 0.054 Å (Scheme 1) it also donates charge (0.248 e) to (P)Fe(HNO).

The reaction pathway associated with Fe–N(H)O bond breaking and subsequent HNO dimerization is much more thermodynamically favorable, by ~44 kcal/mol in Gibbs free energy, than that associated with the H–NO bond breaking and subsequent H_2 formation. This is largely due to the strong thermodynamic driving force of HNO dimerization (ΔG of –44.46 kcal/mol; Table 2). In fact, the ΔG of –4.25 kcal/mol for the decomposition of the Fe–N(H)O bond in the five-coordinate (porphine)Fe(HNO) compound is similar to that for the H_2 formation pathway overall energy of –4.78 kcal/mol. The corresponding data for Fe–N(H)O decomposition and for the H_2 formation pathway are similar for the six-coordinate (porphine)Fe(HNO)L, at –3.30 kcal/mol and –3.19 kcal/mol, respectively. This suggests that the experimentally observed relative preference of H_2 formation in the presence of the axial ligand, versus HNO loss and subsequent dimerization, is not due to thermodynamics alone, but could be due to the kinetic effect of the hydrogen radical formation and dimerization.

The formation and spectral characterization of the Fe–HNO complexes allowed us to probe their N–N bond-forming reactions with external NO, a key coupling reaction step that is at the center of NO detoxification by fungal NO reductases.[19] As described above, the decomposition of the six-coordinate (OEP)Fe(HNO)(5-MeIm) complex generates H_2 and (OEP)Fe(NO) with no evidence of N_2O formation as judged by headspace IR spectroscopy. Interestingly, however, our preliminary results from the reactions of (OEP)Fe(HNO)(5-MeIm) with external NO show clear N_2O formation resulting from an N–N coupling reaction. To verify that N_2O was indeed forming from a coupling reaction involving the bound HNO and external NO, we employed various NO isotopomers (i.e., containing ^{15}N and/or ^{18}O) in these reactions. Our results reveal that the terminal N-atom of the mixed-isotope N_2O product originates from the Fe-HNO moiety, whereas the central N-atom and the O-atom of the N_2O product originate from the external NO reagent (sketched schematically at the top of Fig. 9). The mixed-isotopic N_2O products were identified by their characteristic gas-phase IR spectra.[26] For example, the reaction of unlabeled (OEP)Fe(HNO)(5-MeIm) with external and doubly-labeled $^{15}N^{18}O$ generates $^{14}N^{15}N^{18}O$ (bands at 2185 and 2162 cm^{-1}) as shown in the solid trace in Fig. 9b. The related reaction of (OEP)Fe($H^{15}N^{18}O$)(5-MeIm) with unlabeled NO generates $^{15}N^{14}N^{16}O$ (Fig. 9c, broken line trace; bands at 2195 and 2169 cm^{-1}). Further, the reaction of (OEP)Fe($H^{15}NO$)(5-MeIm) with unlabeled NO generates $^{15}N^{14}N^{16}O$, namely the same reaction product from the (OEP)Fe($H^{15}N^{18}O$)(5-MeIm)/NO reaction.

Our finding that the terminal N-atom of the mixed-isotope N_2O products originate from the Fe–HNO moiety, whereas the central N- and O-atoms originate from external NO is consistent with that predicted by DFT calculations for the related N–N coupling reaction catalyzed by fungal cyt P450nor.[19, 27] The generation of the additional singly labeled (at the N-atom) N_2O isotopomers implies that other pathways may supplement the mixed-isotope Fe–HNO/NO coupling reactions observed in this non-protein system.

Conclusion

In summary, we have demonstrated, experimentally and computationally, varied outcomes for hydride attack at ferric–NO moieties (five- vs. six-coordinate) that result in either Fe–HNO or Fe–H formation. We have also demonstrated varied

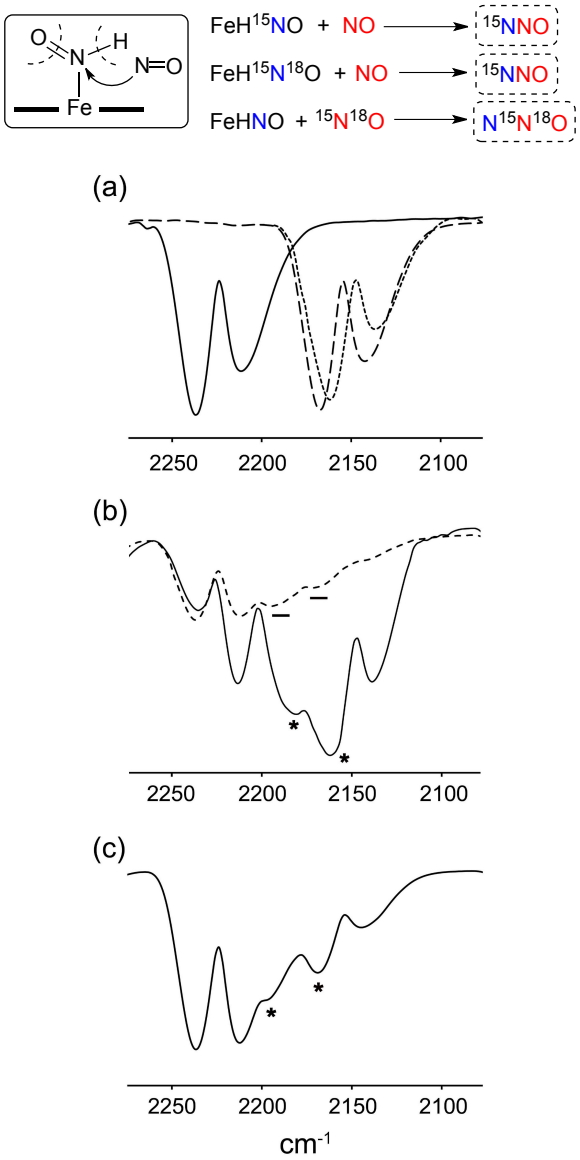

Fig. 9. N_2O formation from the reactions of in situ generated (OEP)Fe(HNO)(5-MeIm) with external NO. (a) spectra of authentic samples of $^{14}N_2O$ (solid line trace, 2237/2212 cm^{-1}), $^{15}N_2O$ (broken line trace, 2167/2142 cm^{-1}), and $^{15}N_2{}^{18}O$ (dotted line trace, 2160/2138 cm^{-1}), (b) spectra of the headspace from the reactions of (*solid line trace*) (OEP)Fe(HNO)(5-MeIm) with $^{15}N^{18}O$, and (*broken line trace*) (OEP)Fe($H^{15}N^{18}O$)(5-MeIm) with NO; the newly formed mixed-isotope N_2O bands are highlighted. The solid line trace shows formation of $^{14}N^{15}N^{18}O$ (2185/2162 cm^{-1}), while the broken line trace shows formation of $^{15}N^{14}N^{16}O$ (2195/2169 cm^{-1}), (c) IR spectrum of the headspace from the reaction of (OEP)Fe($H^{15}NO$)(5-MeIm) with NO. The newly formed bands for the mixed-isotope $^{15}N^{14}N^{16}O$ bands at 2195/2169 cm^{-1} are highlighted. The singly labeled N_2O gases are also present in the headspace, and provide good internal reference spectra.

decomposition pathways for these species, one involving H_2 formation without Fe–N(H)O bond cleavage (to form Fe–NO and H_2) and the other involving Fe–N(H)O bond cleavage (to form N_2O). We have also shown that the Fe–HNO species can react with external NO to generate N_2O in which the central N and the O atoms of N_2O derive from the external NO reagent. These results have set up excellent framework for the study of the Fe–HNO complexes related to their observed biology. Further work to delineate the reaction mechanism of the N–N coupling reactions and related reactions are underway.

Experimental

General

The reactions were performed anaerobically in standard Schlenk glassware and/or in a glove box under a nitrogen atmosphere. Solvents used in the reactions were collected under nitrogen from a Pure Solv 400-5-MD Solvent Purification System (Innovative Technology) or distilled from appropriate drying agents under an atmosphere of nitrogen. Nitric oxide (NO; Air Gas Inc.) gas was passed through a potassium hydroxide column, then through a cold trap (dry ice/acetone) prior to its contact with the precursor solution to avoid the introduction of NO_x impurities. ^{15}NO (Icon Isotope Inc., 99% ^{15}N) was used as received without further purification. FT-IR spectra were recorded on a Bruker Tensor 27 spectrometer. ^1H NMR experiments for Fe–HNO and Fe–H detection were performed on a 400 MHz Varian NMR spectrometer at –20°C and –35°C, respectively. $^{11}B\{^1H\}$ NMR experiments were performed on a 400 MHz Varian NMR spectrometer using quartz NMR tubes.

[(PPDME)Fe(NO)(5-MeIm)]SbF_6

A CH_2Cl_2 (5 mL) solution of [(PPDME)Fe]SbF_6 (13.8 mg, 0.016 mmol) with 1 equiv of 4/5-methylimidazole (1.3 mg, 0.016 mmol) was stirred for 2 h, followed by the introduction of NO gas, in a similar manner to that used to prepare other crystalline $[(por)Fe(NO)(L)]^+$ complexes.[28] X-ray diffraction-quality crystals of the product [(PPDME)Fe(NO)(5-MeIm)]SbF_6 (9.0 mg, 58% isolated yield based on Fe) were obtained from a mixed CH_2Cl_2/methanol solvent system under an NO atmosphere. IR (KBr): υ_{NO} = 1905 cm^{-1}. Characteristic band of uncoordinated hexafluoroantimonate: $\upsilon_{Sb\text{-}F}$ = 659 cm^{-1}.[29]

(PPDME)Fe(HNO)(5-MeIm)

To a $CDCl_3$ (0.5 mL) solution of [(PPDME)Fe(NO)(5-MeIm)]OTf (8.1 mg, 0.009 mmol; υ_{NO} 1912 cm^{-1} ($\upsilon_{^{15}NO}$ 1874 cm^{-1})) in a J. Young NMR tube at –20 °C was added a $CDCl_3$ (0.2 mL) solution of $[NBu_4]BH_4$ (5.0 mg, 0.017 mmol) in a similar manner to that reported by us earlier.[21] The ^1H NMR spectra were recorded immediately. ^1H NMR (–20° C, 400 MHz): 13.93 ppm (s, Fe–*H*NO; $J_{^{15}N\text{-}H}$ = 77 Hz). The characteristic NO stretching frequency of the (OEP)Fe(HNO)(5-MeIm) complex was obtained from a separate reaction in $CHCl_3$ at –20°C (IR υ_{NO} = 1384 cm^{-1}, $\upsilon_{^{15}NO}$ = 1360 cm^{-1}).

The other (por)Fe(HNO)(L) derivatives were generated in a similar manner.

Detection of H_2 from the decomposition of (PPDME)Fe(HNO)(5-MeIm)

The headspace gas of the reaction mixture to generate (PPDME)Fe(HNO)(5-MeIm) described above was collected using a gas-tight syringe after warming the mixture to room

temperature. The headspace gas was then injected into pre-cooled $CDCl_3$ in an NMR tube and the ^1H NMR spectrum was recorded (Fig. S2A). ^1H NMR: 7.26 (s, residual $CHCl_3$), 4.62 (s, dissolved H_2 gas).[30] The data was compared with an authentic commercial sample of 5% H_2/N_2 (Fig. S2B).

Detection of N_2O from the decomposition of (OEP)Fe(DNO)(5-MeIm) and (OEP)Fe(DNO)(1-MeIm)

The headspace gas of the reaction mixture to generate (OEP)Fe(DNO)(5-MeIm) (using $[NBu_4]BD_4$ as the deuteride source) was vacuum transferred to an IR gas cell (10 cm pathlength) after warming the mixture to room temperature. IR (gas phase): υ_{as} (N_2O) = 2237/2213 ($^{15}N_2O$ = 2167/2145) cm^{-1}. ^2H NMR: δ = 2.2 ppm assigned to D_2O which was confirmed by spiking the sample with authentic D_2O. In a separate reaction, formation of the known five coordinate (OEP)Fe(NO) (solution υ_{NO} 1665 cm^{-1}) was also observed during the decomposition of (OEP)Fe(DNO)(5-MeIm). Identical results above were obtained for the decomposition of (OEP)Fe(DNO)(1-MeIm).

[(OEP)Fe(NO)]OTf

In a manner similar to that used to prepare $[(OEP)Fe(NO)]ClO_4$,[23] NO gas was introduced to a CH_2Cl_2 (5 mL) solution of [(OEP)Fe]OTf[1,2] (10.7 mg, 0.015 mmol). X-ray diffraction-quality crystals of the product [(OEP)Fe(NO)]OTf (6.7 mg, 61% isolated yield based on Fe) were obtained from CH_2Cl_2/*n*-hexane under an NO atmosphere. IR (KBr): υ_{NO} = 1856, 1841 cm^{-1}.

(OEP)Fe(NO)H

To a $CDCl_3$ (0.5 mL) solution of [(OEP)Fe(NO)]OTf [7] (7.9 mg, 0.013 mmol; IR υ_{NO} =1856 and 1841 cm^{-1}) in a J. Young NMR tube at –35 °C was added a $CDCl_3$ (0.2 mL) solution of $[NBu_4]BH_4$ (6.0 mg, 0.02 mmol). The ^1H NMR spectra were recorded immediately. ^1H NMR (–35° C, 400 MHz): –4.11 ppm (s, Fe–*H*).

Thermal decomposition of (OEP)Fe(NO)H

IR and ^1H NMR spectroscopy were utilized to monitor the decomposition of (OEP)Fe(NO)H in the product mixture from the reaction of [(OEP)Fe(NO)]OTf with $[NBu_4]BH_4$. The IR spectrum was recorded after warming the solution mixture to room temperature for 0.5 h. IR ($CHCl_3$): υ_{NO} = 1668 cm^{-1}. ^1H NMR (–35° C, 400 MHz): δ 4.62 ppm assigned to the H_2 by-product of the decomposition (see Fig. S2).[6]

Reaction of (OEP)Fe(HNO)(L) with NO and its isotopomers

(a) $^{15}N^{18}O$ gas was introduced to a CH_2Cl_2 (3 mL) solution of the *in-situ* prepared (OEP)Fe(HNO)(5-MeIm) (–95 °C) in a sealed Schlenk tube. The reaction mixture was stirred for 10 min at this temperature. The solution was then slowly warmed to room temperature and stirred for additional 30 min. The headspace gases formed during the reaction were vacuum transferred to a gas IR cell (10 cm path length). IR (gas phase): in addition to the bands due to singly labeled N-atom of N_2O (N_2O at 2237/2213 cm^{-1} and $^{15}N_2{}^{18}O$ at 2160/2137 cm^{-1}), new bands were observed at 2185/2162 cm^{-1} assigned to $^{14}N^{15}N^{18}O$ (the band at 2162 cm^{-1} overlaps with a $^{15}N_2{}^{18}O$ band).

(b) A separate reaction of (OEP)Fe($H^{15}N^{18}O$)(5-MeIm) with NO was also conducted in a similar manner described above. IR (gas phase): in addition to the bands due to singly labeled N-atom of N_2O gases, new bands were formed at 2195/2169 cm^{-1} assigned to $^{15}N^{14}N^{16}O$.

(c) In a similar manner, we conducted a reaction of singly labeled (OEP)Fe($H^{15}NO$)(5-MeIm) with unlabeled NO. in addition to the bands due to N_2O and $^{15}N_2O$, new bands were formed at 2195/2169 cm^{-1} assigned to $^{15}N^{14}N^{16}O$.

Computational Details

All calculations were performed using the program Gaussian 09[31] as reported previously.[21] Full geometry optimizations were conducted for all chemical species studied with subsequent frequency calculations to verify the nature of the corresponding stationary states on their potential energy surfaces and provide zero-point energy corrected electronic energies, enthalpies, and Gibbs free energies. Based on a recent methodology study,[21] geometries were optimized using the mPW1PW91[32] method and the NMR properties were calculated using the B3LYP[33] method with solvent ($CHCl_3$) effect included using the PCM formalism,[34-37] similar to the approach used previously to study ^1H NMR shifts in various organometallic complexes.[38] The basis set used in the geometry optimization is Wachters' basis[39] for iron, 6-311++G(2d,2p) for 1st shell atoms (atoms bonded to iron, HNO, and BH_3/B_2H_6), and 6-31G(d) for other atoms. The basis set used in the NMR calculation is similar with the only difference of using LanL2DZ[40] basis for Fe. The calculated NO frequencies of various iron porphyrin systems studied in this work were scaled using the experimental/computational NO frequency (1380/1568) for a related HNO Ru porphyrin system.[11] The atomic charges were calculated using the Merz-Singh-Kollman scheme[41] as implemented in Gaussian 09.

Notes and references

‡ The crystal structures of $[(PPDME)Fe(NO)(5\text{-}MeIm)]SbF_6$ and [(OEP)Fe(NO)]OTf have been deposited with the Cambridge Structural Database, with ID numbers of CCDC1484724 and CCDC1484725, respectively. Selected data are included in the Supporting Information.

Acknowledgements

We are grateful to the U.S. National Science Foundation (Grants CHE-1213674 and CHE-1566509 to GBR-A) and to the U.S. National Institutes of Health (GM085774 to YZ) for funding for this work. We also thank Jim Cornell for technical assistance with our quartz NMR tubes used for ^{11}B NMR spectroscopy.

References

1. K. M. Miranda, *Coord. Chem. Rev.*, 2005, **249**, 433-455.
2. P. J. Farmer and F. Sulc, *J. Inorg. Biochem.*, 2005, **99**, 166-184.
3. A. L. Speelman and N. Lehnert, *Acc. Chem. Res.*, 2014, **47**, 1106-1116.
4. F. Doctorovich, D. E. Bikiel, J. Pellegrino, S. A. Suarez and M. A. Marti, *Acc. Chem. Res.*, 2014, **47**, 2907-2916.
5. Z. Miao and S. B. King, *Nitric Oxide*, 2016, **57**, 1-14.
6. M. Hamer, S. A. Suarez, N. I. Neuman, L. Alvarez, M. Munoz, M. A. Marti and F. Doctorovich, *Inorg Chem*, 2015, **54**, 9342-9350.
7. D. Bykov and F. Neese, *Inorg. Chem.*, 2015, **54**, 9303-9316.
8. A. Daiber, H. Shoun and V. Ullrich, *J. Inorg. Biochem.*, 2005, **99**, 185-193.
9. I.-K. Choi, Y. Liu, D. Feng, K.-J. Paeng and M. D. Ryan, *Inorg. Chem.*, 1991, **30**, 1832-1839.
10. M. H. Barley, K. J. Takeuchi and T. J. Meyer, *J. Am. Chem. Soc.*, 1986, **108**, 5876-5885.
11. J. Lee and G. B. Richter-Addo, *J. Inorg. Biochem.*, 2004, **98**, 1247-1250.
12. L. E. Goodrich, S. Roy, E. E. Alp, J. Y. Zhao, M. Y. Hu and N. Lehnert, *Inorg. Chem.*, 2013, **52**, 7766-7780.
13. M. R. Kumar, D. Pervitsky, L. Chen, T. Poulos, S. Kundu, M. S. Hargrove, E. J. Rivera, A. Diaz, J. L. Colon and P. J. Farmer, *Biochemistry*, 2009, **48**, 5018-5025.
14. F. Doctorovich, D. Bikiel, J. Pellegrino, S. A. Suarez, A. Larsen and M. A. Marti, *Coord. Chem. Rev.*, 2011, **255**, 2764-2784.
15. J. Pellegrino, S. E. Bari, D. E. Bikiel and F. Doctorovich, *J. Am. Chem. Soc.*, 2010, **132**, 989-995.
16. B. Hu and J. F. Li, *Angew. Chem. Int. Ed.*, 2015, **54**, 10579-10582.
17. N. Kundakarla, S. Lindeman, M. H. Rahman and M. D. Ryan, *Inorg. Chem.*, 2016, DOI: 10.1021/acs.inorgchem.5b02384.
18. D. P. Linder and K. R. Rodgers, *Inorg. Chem.*, 2005, **44**, 8259-8264.
19. C. Riplinger, E. Bill, A. Daiber, V. Ullrich, H. Shoun and F. Neese, *Chem. Eur. J.*, 2014, **20**, 1602-1614.
20. Y. Zhang, *J. Inorg. Biochem.*, 2013, **118**, 191-2000, and references therein.
21. E. G. Abucayon, R. L. Khade, D. R. Powell, Y. Zhang and G. B. Richter-Addo, *J. Am. Chem. Soc.*, 2016, **138**, 104-107.
22. W. R. Scheidt, Y. J. Lee and K. Hatano, *J. Am. Chem. Soc.*, 1984, **106**, 3191-3198.
23. M. K. Ellison, C. E. Schulz and W. R. Scheidt, *Inorg. Chem.*, 2000, **39**, 5102-5110.
24. G. B. Richter-Addo, R. A. Wheeler, C. A. Hixon, L. Chen, M. A. Khan, M. K. Ellison, C. E. Schulz and W. R. Scheidt, *J. Am. Chem. Soc.*, 2001, **123**, 6314-6326.
25. A. Brandstrom, U. Junggren and B. Lamm, *Tetrahedron Lett.*, 1972, 3173-3176.
26. Y. Dubowski, D. Harush and A. Shaviv, *Soil Sci. Soc. Am. J.*, 2014, **78**, 61-69.
27. N. Lehnert, V. K. K. Praneeth and F. Paulat, *J. Comput. Chem.*, 2006, **27**, 1338-1351.
28. M. K. Ellison and W. R. Scheidt, *J. Am. Chem. Soc.*, 1999, **121**, 5210-5219.
29. C. A. Reed, T. Mashiko, S. P. Bentley, M. E. Kastner, W. R. Scheidt, K. Spartalian and G. Lang, *J. Am. Chem. Soc.*, 1979, **101**, 2948-2958.
30. G. R. Fulmer, A. J. M. Miller, N. H. Sherden, H. E. Gottlieb, A. Nudelman, B. M. Stoltz, J. E. Bercaw and K. I. Goldberg, *Organometallics*, 2010, **29**, 2176-2179.
31. M. J. Frisch et al., *Gaussian-09*, Revision B.01; Gaussian Inc., Wallingford, CT, 2010.
32. C. Adamo and V. Barone, *J. Chem. Phys.*, 1998, **108**, 664-675.
33. A. D. Becke, *J. Chem. Phys.*, 1993, **98**, 5648-5652.
34. M. Cossi, V. Barone, R. Cammi and J. Tomasi, *Chem. Phys. Lett.*, 1996, **255**, 327-335.
35. M. Cossi, V. Barone, B. Mennucci and J. Tomasi, *Chem. Phys. Lett.*, 1998, **286**, 253-260.
36. M. Cossi, G. Scalmani, N. Rega and V. Barone, *J. Chem. Phys.*, 2002, **117**, 43-54.
37. B. Mennucci and J. Tomasi, *J. Chem. Phys.*, 1997, **106**, 5151-5158.
38. Y. Zhang, J. C. Lewis, R. G. Bergman, J. A. Ellman and E. Oldfield, *Organometallics*, 2006, **25**, 3515-3519.
39. A. J. Wachters, *J. Chem. Phys.*, 1970, **52**, 1033-1036.
40. P. J. Hay and W. R. Wadt, *J. Chem. Phys.*, 1985, **82**, 270-283.
41. B. H. Besler, K. M. Merz and P. A. Kollman, *J. Comput. Chem.*, 1990, **11**, 431-439.

